



## VIBRATION CHARACTERISTICS OF STEEL BUILDINGS BASED ON LARGE SHAKING TABLE TESTS AT E-DEFENSE

T. Tojo<sup>(1)</sup>, N. Nakamura<sup>(2)</sup>, K. Kajiwara<sup>(3)</sup>, N. Satake<sup>(4)</sup>, Y. Tosauchi<sup>(5)</sup>

<sup>(1)</sup> *Researcher, Takenaka Corporation, toujou.takaki@takenaka.co.jp*

<sup>(2)</sup> *Professor, Hiroshima University, naohiro3@hiroshima-u.ac.jp*

<sup>(3)</sup> *Director, National Research Institute for Earth Science and Disaster Resilience, kaji@bosai.go.jp*

<sup>(4)</sup> *Engineer, Engineering & Risk Services Corporation, satake@ers-co.jp*

<sup>(5)</sup> *Researcher, Fujita Corporation, yusuke.tosauchi@fujita.co.jp*

### **Abstract**

Natural period and damping ratio are important values in seismic design. Recently, many of the findings for these values have been obtained from earthquake observation records and recommended values of the vibration characteristics have been proposed for buildings [e.g. 1]. However, the observation records of buildings are affected by the soil–structure interaction in addition to structural and nonstructural members. Therefore, only the characteristics of the building structure remain unclear. This study focused on the structural vibration characteristics by using the records of large shaking table tests. Previously, we evaluated changes in vibration characteristics depending on the deformation level of the main structure for reinforced concrete (RC) specimens. In this study, we continued the previous study and evaluated steel specimens subjected to strong input motion. The experimental data were analyzed using the autoregressive exogenous (ARX) model. Moreover, the effects of the experienced largest deformation on the vibration characteristics for these RC and steel specimens were investigated.

In this study, three specimens (Specimen St.1–3) simulating a steel anti seismic building were studied mainly. Specimens St.1, St.2 and St.3 had 4, 5, and 3 stories, respectively. Their respective natural periods were approximately from 0.8 to 0.6 s. The examination objects of their input motions were three types of excitation waves: random, scaled, and ground motion excitations.

The identification results of the natural period and damping ratio of the first and second modes in the horizontal direction were studied. The ARX model with a one-input one-output system was used as an identification scheme. The experimental data, published from the National Research Institute for Earth Science and Disaster Resilience were applied to band pass filters. The data of some steel specimens were corrected using the rocking motion of the shaking table.

First, the relation between structural damage and inter-story drift angle were studied for steel specimens. Then, the natural period and damping ration of the first and second modes were studied using all excitations for each specimen. The amplitude dependencies of each vibration characteristics were also studied in detail. Finally, the relation between the experienced largest deformation and these vibration characteristics were investigated.

The following main results were obtained:

- 1) The first and second mode damping ratios for the three types of steel specimens were approximately 1%–3% in elastic range. The result showed a slight variability in these values and roughly agreed with the recommended values in Japanese seismic design.
- 2) The natural period had an amplitude dependence increasing the value according to the increasing deformation for both of RC and steel specimens. For steel specimens, the damping ratio had an amplitude dependency, increasing the value according to the increasing deformation to a certain drift angle. After that, the value decreased with increasing deformation. These amplitude dependency was observed regardless of the foundation conditions (on a shaking table for this study).
- 3) In the relation between each vibration characteristics and experienced maximum drift angle, the changes in the values of steel specimens were relatively small compared with those of RC specimens.

*Keywords: Natural period, Damping ratio, Anti seismic building, Amplitude dependence, Large shaking table*



## 1. Introduction

Knowledge of a building's vibration characteristics, such as natural period and damping ratio, is indispensable for estimating its behavior and seismic performance during an earthquake. A previous study has recommended values of natural periods (natural frequencies) and damping ratios in the elastic design ranges of mid-to-high-rise reinforced concrete (RC) and steel buildings based on extensive analyses of excitation tests and observations until 2000 [1]. In the case of an overseas structure, the damping ratio remains constant up to a certain building height and thereafter decreases as the height increases [2]. Fig. 1 shows the recommended damping ratios of RC ( $h_{RC}$ ) and steel ( $h_S$ ) buildings from the aforementioned studies [1, 2], and an average inter-story height of 3.3 m is assumed for comparison as given in [2]. These recommended values are affected by soil-structure interactions (SSIs). Therefore, the damping ratios increase with decreases in the heights of the buildings. It is important that the vibration characteristics of buildings itself without SSI effects were investigated. Moreover, one cannot deny the possibility that these buildings may experience earthquakes beyond the current design levels. However, the recommended damping ratios are used in structural designs even though a building's response may attain ultimate deformation levels. Thus, it is also important to survey the vibration characteristics of the building's response when it attains ultimate deformation level.

More recently, spurred by the 2011 Earthquake off the Pacific Coast of Tohoku (hereafter referred to as the 3.11 Earthquake), several studies have reported gradual changes in the natural period and damping ratio prior to the 3.11 Earthquake and differences in the values before and after the earthquake in buildings of various structural types. The pattern of changes in vibration characteristics associated with vibration amplitudes (called amplitude dependence) during the 3.11 Earthquake and its minor shocks have been studied [e.g. 3, 4]. Although many observation records were obtained and analyzed those studies, there were very few records for buildings that attained ultimate deformation levels. To determine the variable factors of vibration characteristics of buildings, it is necessary to analyze and evaluate the trends from actual data that are measured under equivalent conditions and independent of the type of structure.

The 3-D Full-Scale Earthquake Testing Facility at the National Research Institute for Earth Science and Disaster Resilience (NIED) (popularly called as E-Defense, having a 15 m × 20 m shaking table and maximum load specification of 1200 t) can accommodate tests for full-sized building specimens indoors. Many excitation tests ranging from micro-deformation to ultimate deformation levels were performed on numerous RC and steel structural specimens that were designed in accordance with the Japanese seismic design standards, and these data have been publicly released [5]. As a result, it is possible to perform evaluations ranging from micro-deformations to ultimate failure without SSI effects, which take into account changes in structural soundness and vibration characteristics under the current design code.

In a previous work, we evaluated changes in vibration characteristics based on the deformation levels of the main structures of RC and steel buildings from the results of multiple specimens tested at E-Defense [6, 7]. In this study, we have continued their evaluations from the previous work and performed similar assessments on steel buildings by adding new analysis results to the contents published in the reference [7].

To summarize, in this study, vibration characteristics such as the natural period and damping ratio for each structural specimen are identified, and our findings, including those for the first- and second-order modes, are presented using a unified method for all specimen types. Specifically, the ARX model [e.g. 8] used in references [6, 7] is employed to analyze the vibration characteristics and their changes during, before, and after excitation; further, the maximum deformations experienced by the specimens and their effects on the vibration characteristics are summarized.

## 2. Outline of specimens and excitation wave

In this study, earthquake-resistant structural specimens that simulate three steel buildings (specimens St.1 to St.3) are examined. The configurations of the specimens are shown in Fig. 2. Table 1 shows the data for each specimen. All specimens are in full-scale, with the first natural periods in the table calculated from the initial



random excitation [9–13] (for specimen St.3, the described natural period is in the Y direction alone, since the shaking test was in one direction only). The excitation wave in the tests is classified by the type of excitation: random excitation (to determine vibration characteristics), scaled excitation (lower level ground motion excitation), and ground motion excitation. All these excitation results were considered in this study. Table 2 shows the ground motion excitation and the maximum story drift angle in both X and Y directions during the motion for each specimen, taken from tables or graphs given in previous studies [9–13]. For the tests on specimens 1 and 2, the JR- Takatori wave, observed during the Great Hanshin Earthquake, was used as the ground motion excitation. For the specimen St.3 tests, the input excitations used were the JR- Takatori wave and the simulated Nankai Trough wave as unidirectional shaking in the Y direction. Table 2 shows the definition of their deformation level stage  $S_1$ – $S_4$  according to the amplitude level (details are described in section 4.1) and damage state for each specimen after the ground motion excitations.

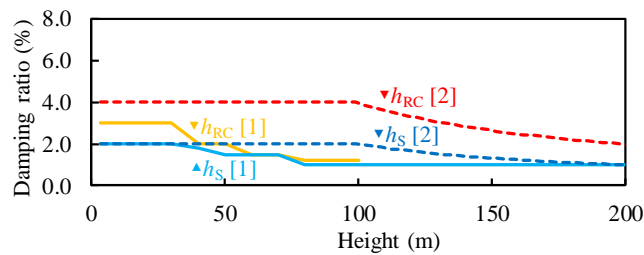


Fig. 1 – Recommendations of damping ratio in references [1, 2]

◆ Acceleration sensor

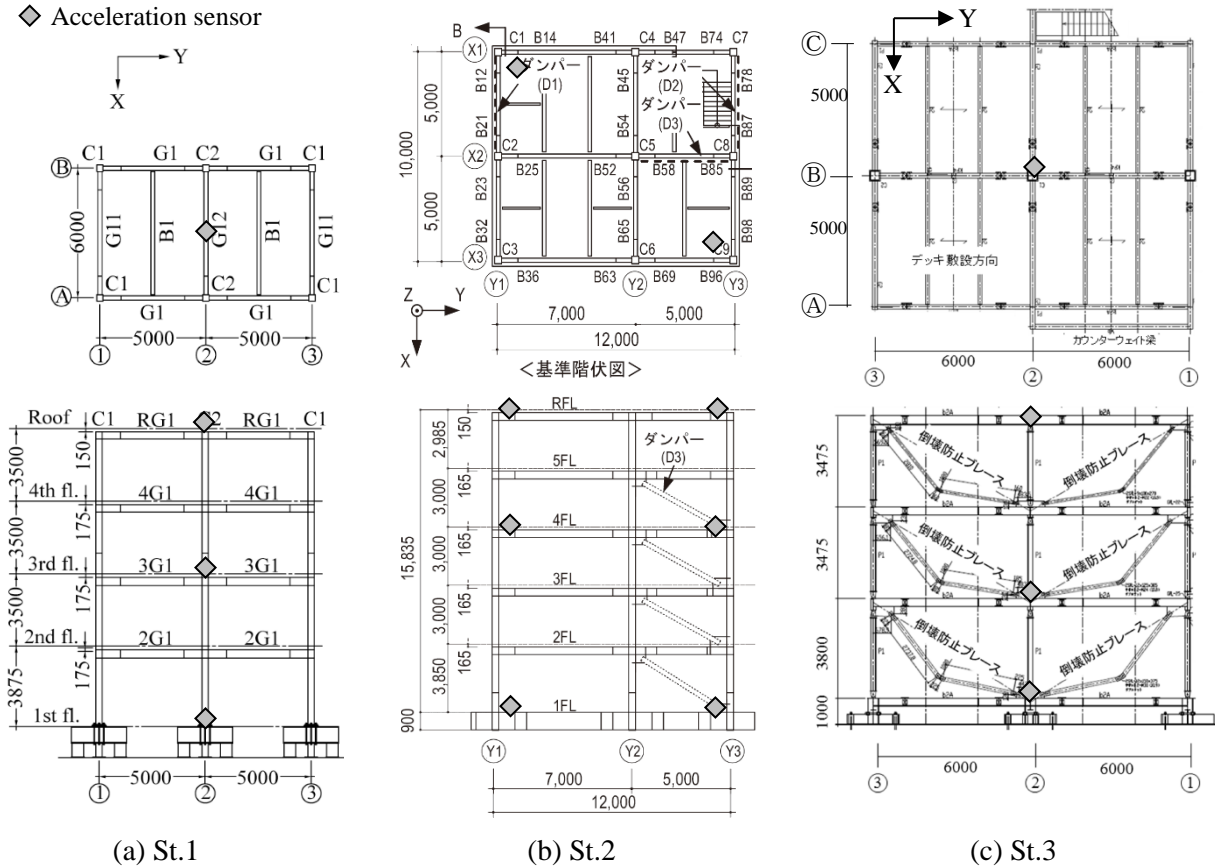


Fig. 2 Configuration of Specimen St.1–3



Table 1 Specimen data

Specimen	Story	Height (m)	Weight (ton)	first natural period (s)		Scale
				X <sup>†</sup>	Y	
St.1	4	14.375	219	0.82	0.78	Full
St.2	5	15.835	498	0.66	0.69	
St.3	3	10.750	196	-	0.64	

<sup>†</sup>for specimen St.3, the described natural period is in the Y direction alone, since the shaking test was in one direction only.

Table 2 Maximum story drift angle and definition of deformation level stage

Specimen	Excitation wave	Maximum story drift angle $R_{max}$ ( $\times 10^{-3}$ rad)		Deformation level stage and damage state after experienced excitation	
		X	Y	Stage	Damage state
St.1	JR-Takatori-5%	1.2	1.1	S <sub>1</sub>	damage in exterior cladding
	JR-Takatori-10%	2.6	2.4		
	JR-Takatori-13%	2.6	2.8		
	JR-Takatori-20%	6.0	5.0	S <sub>2</sub>	yield main frame
	JR-Takatori-40%	10.0	11.0		
	JR-Takatori-60%	14.0	19.0		
	JR-Takatori-100%	91.4	152.4		
St.2	JR-Takatori-5%	0.7	0.5	S <sub>1</sub>	(damages in exterior cladding and slab before the stage, S <sub>1</sub> )
	JR-Takatori-20%	3.5	2.0		
	JR-Takatori-30%	4.8	3.5		
	JR-Takatori-40%	5.5	5.7	S <sub>2</sub>	yield main frame
	JR-Takatori-50%	7.0	7.4		
	JR-Takatori-70%	11.0	8.4		
St.3	Nankai-50%	-	5.4	S <sub>1</sub> ~S <sub>2</sub>	damage in slab
	Nankai-100%	-	12.7		
	JR-Takatori-40%	-	15.2	S <sub>3</sub>	yield main frame
	JR-Takatori-60%	-	28.4		
	JR-Takatori-80%	-	30.7		
	JR-Takatori-100%	-	76.5		
	Nankai-50%	-	13.9		
	Nankai-100%	-	24.5	S <sub>4</sub>	-
	Nankai-150%	-	31.2		



## 2.1 Specimen St.1 [9–11]

Specimen St.1 in Fig. 1 (a) simulates a four-story building with a height of about 14.4 m. Tests were conducted on this specimen with the objective of confirming the structural performance and degree of damage when the building is subjected to the level of earthquake motions assumed in the current design codes. Moreover, the tests were performed to determine the margin at which the building completely collapses under seismic motions with large amplitude levels. Simultaneously, it is important to note that nonstructural members were attached inside and outside the test building in imitation of the actual building in order to evaluate its capacity to retain building functions.

## 2.2 Specimen St.2 [12]

Specimen St.2 in Fig. 1 (b) simulates a five-story building with a height of about 15.8 m. Similar to specimen St.1, non-structural members were provided to match the actual conditions as much as possible, assuming the example of an office building. For the tests, brace dampers were used as damping devices, since the objective of the study was to verify the performance of buildings with damping devices attached under large earthquakes. Excitation tests were conducted in their respective order on the same specimen, with (1) steel, (2) viscous, (3) oil, and (4) viscoelastic dampers, as well as with (5) no damper attached. In this study, only the test results of case (5), with no damper attached, are considered. In case (5), the main structure had already experienced multiple excitations performed with the damper in each of the cases (1) to (4), although the structure remained within the elastic range. However, cracks had appeared on the slabs and the stiffness had already decreased as a result during the tests performed in cases (1) to (4). Hence, the value given in Table 1 is the natural period for the initial state for case (5).

## 2.3 Specimen St.3 [13]

Specimen St.3 in Fig. 1 (c) simulates a structural plane of a three-story building frame with a height of about 11 m. However, this specimen is somewhat different from the usual building conditions. The columns on line A and C in the longer direction support the floor slabs in the vertical direction alone. The column top and column base at each floor are pin-supported, so as not to resist lateral forces, while the first floor column bases on B are exposed with only the column bases on B fixed. The main objective of the tests on this specimen was to establish a method to evaluate the residual seismic performance of damaged buildings, with a focus on continuing the use of buildings with damaged main structural members. During the input of the JR- Takatori wave 100% (shown in Table 2), the beam end fracture was confirmed, despite several excitations continuing even after the rupture, in accordance with the objective given above.

## 3. Identification method for vibration characteristics

In this study, the results obtained from identifying the vibration characteristics, namely the first and second-mode natural periods and damping ratios in the horizontal direction, are analyzed for each specimen. The ARX model [8] is used as the identification method, with a single input and single output system and a band-pass filter applied beforehand on the input-output data [3, 4].

Publicly available data from NIED was used to examine actual measurement data [5]. During identification, acceleration records in the horizontal direction on the first and top floors of the building were used to identify the first mode, whereas the records on the first and middle floors of the building are used to identify the second mode. The locations of the accelerometers are shown in Fig. 2. For specimen St.2, the average value of the two points is used.

For specimen St.2, it has been reported in the reference [14] that the effect of the shaking table's rocking motion is relatively large, such that the rotational acceleration component cannot be ignored. To identify the vibration characteristics in the referenced study, the transfer function is defined by the following equation as the ratio of the absolute acceleration response at the  $k$ -th floor  $\ddot{u}_{tot,k}$  and the harmonic acceleration input corresponding to the  $j$ -th mode  $\ddot{u}_g + H_{eq,j} \ddot{\theta}_g$



$$G_{k,j}(\omega) = \frac{\ddot{u}_{tot,k}}{\ddot{u}_g + H_{eq,j} \ddot{\theta}_g} \quad (1)$$

Here,  $H_{eq,j}$  is the equivalent height for the  $j$ -th mode. In the reference [14], the vibration characteristics were identified by matching the theoretical transfer function obtained assuming the transfer function in Eq. (1) to the spectral ratio of the actual measured data determined by similarly considering the rotation.

Accordingly, the input data used for identifying specimen St.2 in this study is calibrated in advance by considering table-rocking motion according to Eq. (1). We consider the rotation effect for identifying specimen St.1 as well. However, for specimens St.3, no particular calibration was performed, as the rotation effect can be considered small, since the specimens are lightweight [15].

After verifying that the solution is stable and that the effect of parameter changes on the identification results is small, the analysis conditions of the ARX model [8] are set as follows for all specimens.

- The resampling is performed at an interval 10 times the time increment of the record.
- The calculation segment is set to 10 s for the JR- Takatori wave, which is characterized by strong pulses, and 20 s for the other excitations. The calculation segment is run at a 1/4 s pitch.
- In principle, the model order is set to two, although it is set to four only when damage has progressed, and the identification accuracy is not stable with two orders.
- The time delay term is not considered.

As is shown in the discussion below regarding the vibration characteristics of each specimen, the natural period (frequency) changes as the amplitude level rises and the damage progresses in the specimens. Thus, for the preset band-pass filter, the transfer function of each excitation is verified, and a trapezoidal filter is determined such that the peak of each mode is enveloped, according to the damage process as in the references [3, 4].

#### 4. Discussion on amplitude dependence

In this section, the amplitude dependence of the natural period and damping ratio and their change patterns according to the structural damage are examined in detail. Specimens St.1 and St.3 are studied mainly, because they have a large number of excitations and their changes in vibration characteristics are relatively distinct.

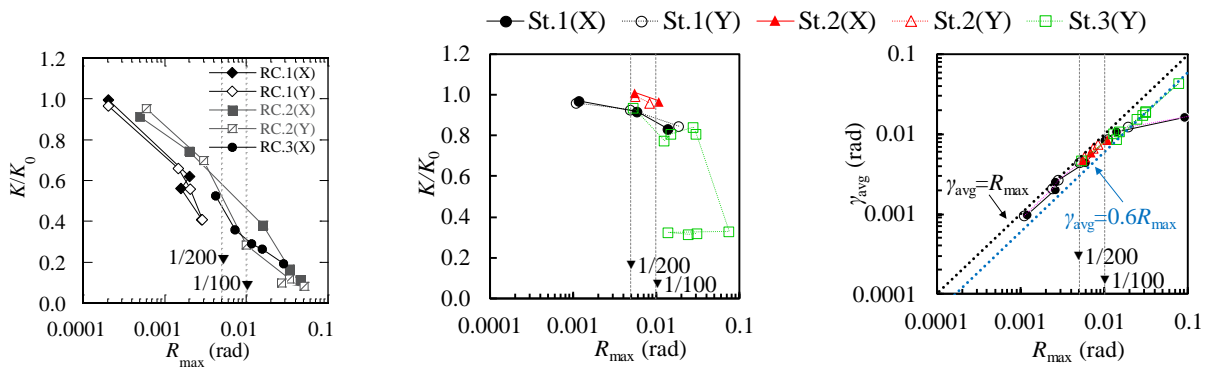


Fig. 3 Relationship between stiffness decline rate  $K/K_0$  and maximum story drift angle  $R_{max}$  of RC specimen [6]

Fig. 4 Relationships between stiffness decline rate  $K/K_0$ , maximum story drift angle  $R_{max}$  and average drift angle  $\gamma_{avg}$

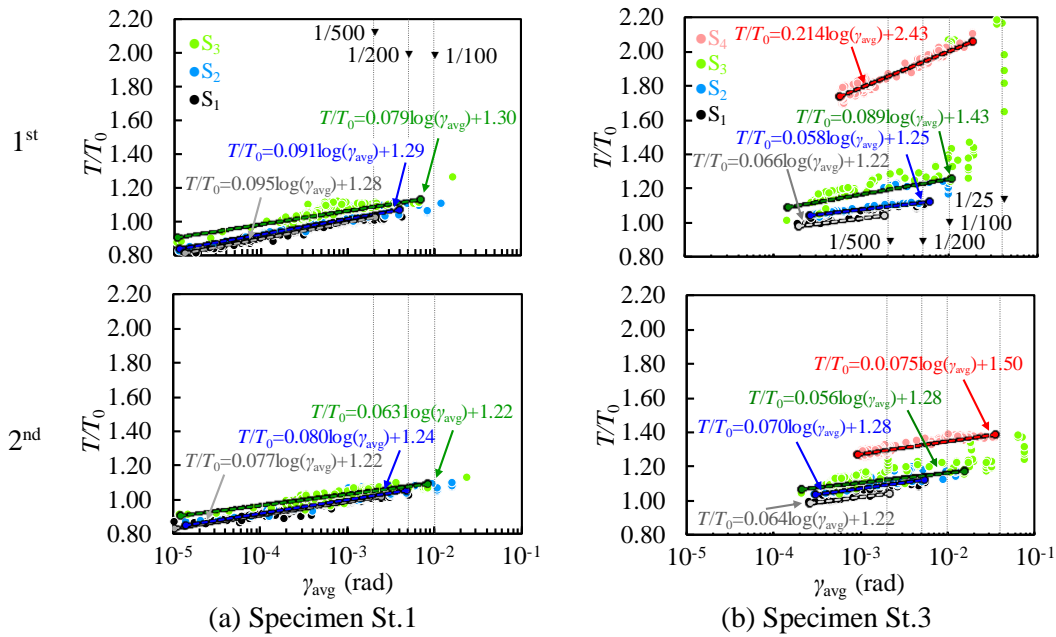


Fig. 5 Relationship between natural period  $T$  and average drift angle  $\gamma_{\text{avg}}$  (upper:1<sup>st</sup> mode, lower:2<sup>nd</sup> mode)

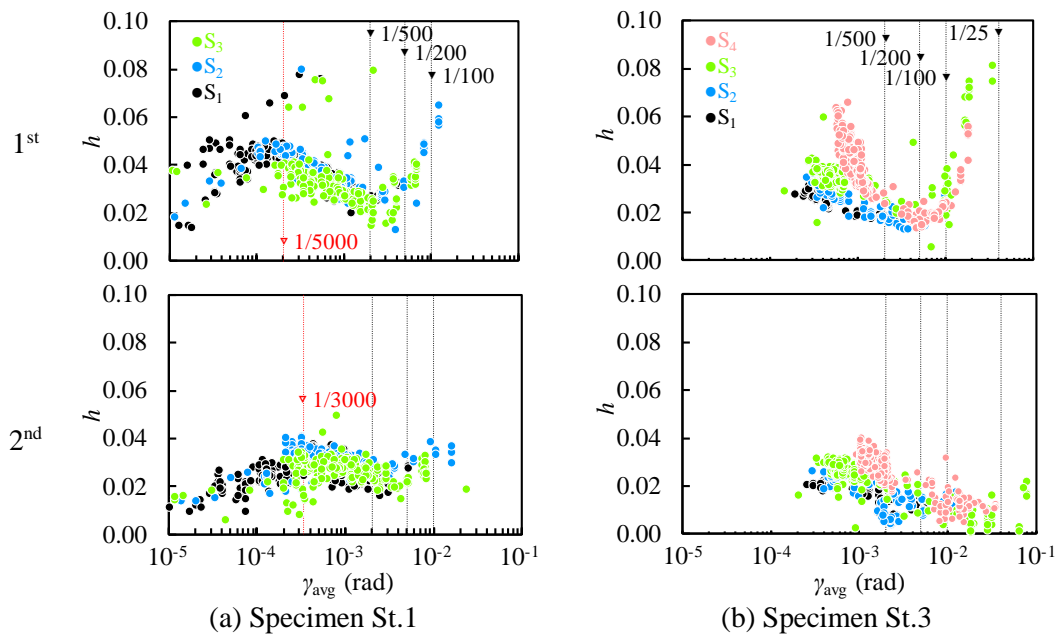


Fig. 6 Relationship between damping ratio  $h$  and average drift angle  $\gamma_{\text{avg}}$  (upper:1<sup>st</sup> mode, lower:2<sup>nd</sup> mode)

#### 4.1 Relationship between structural damage and deformation level stage

Fig. 3 shows the relationship between stiffness decline rate  $K/K_0$  and the maximum story drift angle  $R_{\text{max}}$  of RC specimen [6]. Fig. 4 shows the relationships between stiffness decline rate  $K/K_0$ , the maximum story drift angle  $R_{\text{max}}$  and first mode maximum average drift angle  $\gamma_{\text{avg}}$  for each ground motion excitation. The average drift angle is defined as the value obtained by dividing the maximum relative displacement between the input and output points by their height. The stiffness decline rate was calculated by secant rigidity during the random excitation before and after the ground motion excitation, as in the reference [6].



As shown in Fig. 3, for the RC specimen, it can be seen that the stiffness greatly decreases with increasing the amplitude from the story drift angle  $R_{\max} = 1/1000$  rad or less. On the other hand, for steel specimens, there is little decline in the values until the amplitude exceeded the maximum story drift angle  $R_{\max} = 1/200$  rad in Fig. 4 (a). From previous studies, others [9–13] inferred that the main frames were in the elastic range but non-structural members were damaged at the point. When the value of  $R_{\max} = 1/100$  rad was exceeded, their rigidity decreases for all the specimens. The former is the threshold when taking damage in interior and exterior cladding materials into account, while the latter is almost agreed with the threshold relaxed due to measures taken beforehand to prevent damage to the interior and exterior cladding materials, which are used in the allowable stress calculation in Japanese design code. For only specimen St.3, the stiffness decline rate greatly decreases to the value of about 0.3 because of the beam fractures.

Comparing the story drift angles and average drift angles in Fig. 4 (b), the ratio of  $R_{\max}$  and  $\gamma_{\text{avg}}$  is nearly 1 for both figures until about  $R_{\max} = 1/100$  rad, indicating that the first mode tends to dominate. Beyond that,  $\gamma_{\text{avg}}$  is about 60% of  $R_{\max}$ , because yielding has progressed for all the specimens.

The above results suggest that all the specimens show similar patterns of the relation between the structural damages and maximum story drift angle. Moreover, as an approximation, the vibration characteristics change according with the damage of non-structural member or main structure yields shown in Table 2, when the structure experiences deformations of around  $R_{\max} (= \gamma_{\text{avg}}) = 1/200$  to  $1/100$ . Hence, we classified into three or four deformation level stages,  $S_1$  to  $S_3$  (or  $S_4$ ) below, which is shown in Table 2. The amplitude dependence of the following vibration characteristics is considered by focusing on the changes for each defined stage.

$S_1$ : Until the excitation where the average drift angle experienced by the specimen exceeds  $\gamma_{\text{avg}} \approx 1/200$  rad.

$S_2$ : After  $S_1$ , until the excitation where  $\gamma_{\text{avg}} \approx 1/100$  rad is exceeded.

$S_3$ : After  $S_2$ , until the final excitation where the story collapses for specimen St.1; until the beam fractures for specimen St.3 (until  $\gamma_{\text{avg}} \approx 1/25$  rad is exceeded).

$S_4$ : After  $S_3$ , until the final excitation (for specimen St.3 only).

## 4.2 Natural period

The relationship between the average drift angle  $\gamma_{\text{avg}}$  per excitation segment and the first and second-mode natural period  $T$  under all the excitations are shown in Fig. 5 (a) for specimen St.1 and in Fig. 5 (b) for specimen St.3. The periods are shown as natural period ratios with respect to the average period of the initial random excitation,  $T_0$ . Since the pattern of changes in the X and Y directions of specimen St.1 are similar, only the Y direction is shown. The regression line and approximation at each stage (calculated assuming the micro-deformation range reaching to about  $1/500$  rad for  $S_1$ ), determined as the deformation at which a new maximum average drift angle is experienced at the previous stage and below, are included in the similar color as the graph keys. Their coefficient of determination  $R^2$  is stable and the value of about 0.8 to 0.9.

First, specimen St.1 was considered. From Fig. 5 (a), the overall trend of amplitude dependence can be observed. Here, the natural period ratio increases with increasing drift angles, regardless of progress of damage in both first and second mode periods. The changes from stages  $S_1$  to  $S_3$  in (a) of the figure were examined. First, for  $S_1$ , both first and second-mode natural period ratios vary with generally constant slopes until the average drift angle reaches a maximum of  $1/200$  rad and exterior cladding is damaged. For  $S_2$ , the same degree of amplitude dependence as  $S_1$  was generally maintained until reaching drift angles of about  $1/100$  rad and showing relatively pronounced yielding. After shifting to  $S_3$ , the lengthening of the periods became slightly more distinct, with a maximum of about 10% compared with  $S_1$ .

Next, the results for specimen St.3 were considered. From Fig. 5 (b), an overall trend of amplitude dependence similar to specimen St.1 can be observed in all stages, regardless of the degree of damage. However, the following differences can be seen in the progression from stages  $S_1$  to  $S_3$  ( $S_4$ ). Looking at the first-mode period ratio in (b) of the figure, the change in amplitude dependence (slope) is relatively small as the stages shift from  $S_1$  to  $S_2$ , similar to specimen St.1. In contrast, as the stages shifted from  $S_2$  to  $S_3$ , the first-mode period ratio becomes conspicuously large, with around 20%–30% larger approximation values than  $S_1$ , and larger rate of



increases for overall period variation. For specimen 3, the yielding of the main structure is slight, while the cracks on the slab have propagated considerably [13]. This may be the main reason for the larger rate of increase of the natural period ratio from  $S_1$  to  $S_3$  and the more pronounced amplitude dependence than specimen St.1. Furthermore, drift angles of about  $1/25$  rad are reached at  $S_3$ , and the beam on the second floor fractures, hence the shift is made to  $S_4$ .

Considering the change in vibration characteristics of steel structures, a previous study has highlighted the fact that the effect of the floor slab composite action is large [16], and comparison between specimens St.1 and St.3 leads to the assumption that the effects of damage in concrete materials, such as slabs, manifest relatively easily in terms of the amplitude dependence as well.

### 4.3 Damping ratio

Fig. 6 (a) and (b) shows the relationship between the average drift angle  $\gamma_{\text{avg}}$  and the first and second-mode damping ratio  $h$  for specimens St.1 and St.3, respectively. The stage classifications  $S_1$  to  $S_4$  in the key are the same as in Fig. 5. For specimen St.1 in (a) of the figure, the damping ratio appears to increase and decrease depending on the amplitude, with the visually determined boundary line depicted by the symbol  $\nabla$ .

First, the damping ratios of specimen St.1 were considered. From Fig. 6 (a), the overall trend shows a tendency for the values of the damping ratio to become somewhat large in response to increasing amplitude within the deformation range of about around  $1/5000$  to  $1/3000$  or less. In contrast, when the above amplitudes are exceeded, the values tend to decrease within the deformation range of about  $1/200$  rad or less. When the drift angle exceeds about  $1/200$  rad, the values of the damping ratio markedly increase, especially for the first mode. However, this may be considered to be the effect of hysteresis damping due to yielding.

Next, specimen St.3 was considered. From Fig. 6 (b), the amplitude dependence found in specimen St.1, where the values decrease depending on the amplitude, can similarly be observed at each stage below drift angles of about  $1/200$  to  $1/100$  rad. Moreover, the differences between stages  $S_1$  to  $S_3$  for specimen St.1 and St.3 were examined. Overall, both first and second-mode damping ratios tend to increase when comparing values from  $S_1$  to  $S_2$ , and then to  $S_3$  for specimen St.3, while the changes is relatively small in specimen St.1. As pointed out in the changes within the natural period, this difference may be attributed to the cracking of slabs, which causes damping to increase. Furthermore, the values from  $S_3$  to  $S_4$ , which involved beam fracture, also tend to increase in the same way.

Based on the results for specimens St.1 and St.3 above, the change in the amplitude dependence of the damping ratio shows a common tendency to decrease as the amplitude increases, regardless of the amount of non-structural members. For both first and second orders of both specimens, the difference in values from  $S_1$  to  $S_3$  ( $S_4$ ) tend to be relatively small at about 2% when drift angles of about  $1/100$  rad are reached. Then yielding becomes pronounced resulting in large increases in the values. The specimen St.1 which does include non-structural members appears the tendency to increase the amplitude. The amplitude dependence observed largely in the elastic deformation range above has also been reported in a past study analyzing wind observation records [17]. Previous studies have shown that this phenomenon is generally captured by assuming a non-structural wall, which contributes to the stiffness of the entire building up to a certain amplitude, and using an equivalent viscous damping (stick-slip model) that represents the energy consumption due to external friction of the member. Specimen St.1 has many non-structural members, such as inner and outer cladding, which may have also contributed to the rise and fall of the damping ratio.

## 5. Change according to the average drift angle experienced

Chapter 4 show the tendency for natural periods and damping ratios to vary overall, according to the progress of yielding and damage in non-structural members once a certain deformation level is reached. In this section, the relationship between the change in vibration characteristics discussed above and the deformation levels experienced by specimens St.1 to St.3 will be examined. In particular, the focus will only be on random and scaled excitations, with relatively small inputs before and after the main ground motion excitations for each



specimen. The relationships between the maximum of the average drift angles experienced at that point in time will be presented under each excitation and each vibration characteristic.

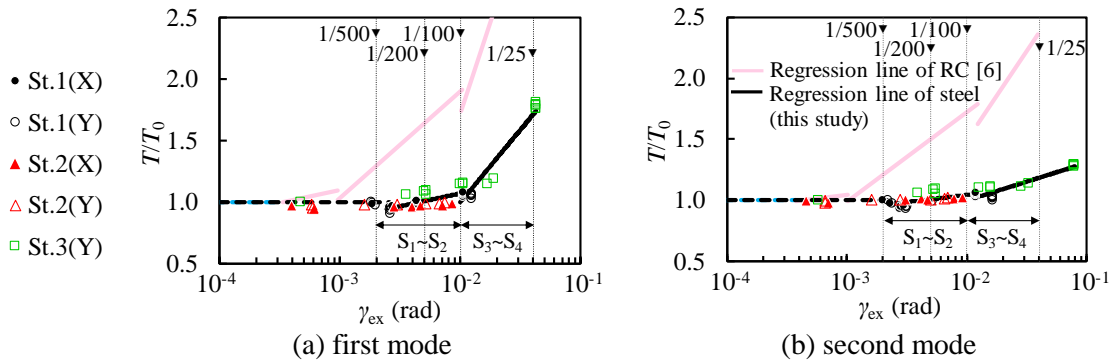


Fig. 7 Relationship between experienced average drift angle  $\gamma_{ex}$  and natural period ratio  $T/T_0$

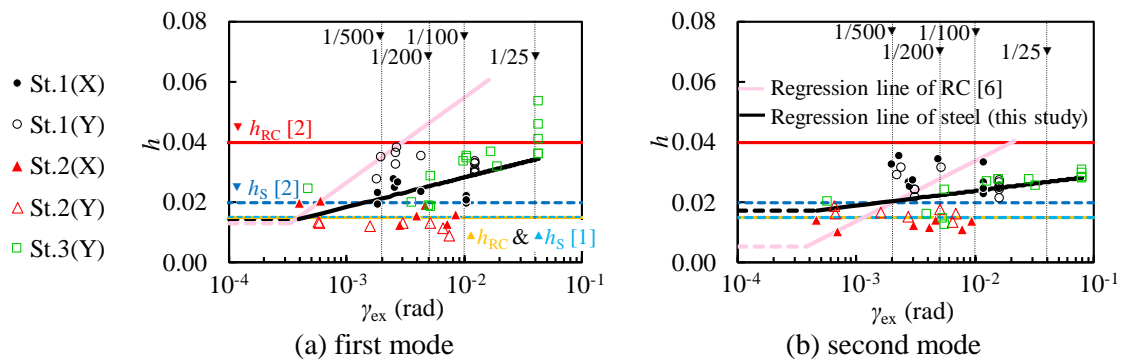


Fig. 8 Relationship between experienced average drift angle  $\gamma_{ex}$  and damping ratio  $h$

## 5.1 Natural period

The relationship between the natural period ratio  $T/T_0$  and the average drift angle experienced  $\gamma_{ex}$  obtained in the X and Y directions for all specimens in the first and second modes are shown in Fig. 7 (a) and (b), respectively. Here, each natural period is obtained as the average value of all relevant excitation segments for each excitation, and it is normalized with respect to the period during the initial random excitation,  $T_0$ . For reference, the regression lines determined from the relationship between the natural period ratio and the drift angle experienced, for the ranges  $S_1$  to  $S_2$  and  $S_3$  to  $S_4$ , based on the four stage classifications defined in Section 4.1, are included in each figure together with the regression lines for the same relationship of three RC specimens in a previous study [6].

According to Fig. 7 (a) and (b), when the specimens experience drift angles of about 1/500 to 1/100 rad, the first and second-mode natural period ratios show a tendency to increase for specimen St.3, where the slab is damaged. They show little change for the other specimens. Compared with the regression lines of the RC specimens [6] in the same range the rates of increase of the period for steel specimens St.1 to St.3 are relatively small. Moreover, the experienced deformation levels at which the period ratio begins to increase are about 1/1000 rad for RC. A relatively large change in gradient can be confirmed, in contrast to which, the drift angles experienced for steel are about 1/100 rad. All the specimens showed pronounced period lengthening, with differences in deformation levels of about a factor of 10.



The studies in the references [3, 4] have compared the amplitude dependence of the natural period before and after the 3.11 Earthquake for many buildings. Herein, it was suggested that steel buildings tend to have smaller changes in amplitude dependence compared with RC buildings, which is almost agreed with the results above.

## 5.2 Damping ratio

The relationship between the first and second-mode damping ratios and the average drift angle experienced are shown in Fig. 8 (a) and (b), respectively. Similarly to the damping ratio, a single value is obtained for each excitation as the average of all segments. As in the previous section, regression lines obtained for the steel structure specimens and for an RC specimen (one specimen only) [6] are likewise included. One regression line was calculated for the results of all stages. However, its coefficient of determination  $R^2$  is value of about 0.2 to 0.3 and show large variations among individual steel specimens. The damping ratio recommended in references [1, 2] for the elastic range is also shown in the figure as  $h_{RC}$  and  $h_S$  respectively.

According to Fig. 8 (a) and (b), when the specimens experience drift angles of about 1/200 rad, the first and second-mode damping ratios show a tendency to increase for specimen St.3, similarly as with the natural period ratio. Moreover, they show generally constant or gradually decreasing values for the other specimens. When the specimens experience drift angles of about 1/100 rad, yielding progresses in all the specimens. However, the change in the damping ratio is small even for specimen St.3, until drift angles of about 1/25 rad are reached. Looking at the change in regression lines, different damping characteristics are found for RC and steel specimens. The damping values of steel and RC specimens are about 1 to 2% and 1 to 3%, respectively until reaching drift angles of about 1/500 rad. These damping ratio almost agree with the recommended values in references [1, 2]. When the drift angle reaches at 1/100 to 1/25 rad, the damping values of the steel specimen is about 3 to 4%, which is about 0.5 to 0.7 times to the RC specimen.

## 6. Conclusions

In this study, the change in vibration characteristics, specifically the horizontal first-mode and second-mode natural periods and damping ratios, were examined using shaking table tests of steel buildings conducted on the E-Defense. In particular, a detailed study was conducted on the change in vibration characteristics according to the deformation level experienced. The findings of the study are as follows.

- The first and second mode damping ratios for the three types of steel specimens were approximately 1%–3% in almost elastic range. The result showed a slight variability in these values and roughly agreed with the recommended values in recommended values of Japanese seismic design [1].
- The natural period had an amplitude dependence increasing the value according to the increasing deformation for steel specimens as well as RC specimens. The effect on amplitude dependence is largely due to damages in a slab. For steel specimens, the damping ratio had an amplitude dependence, increasing the value according to the increasing deformation to a certain drift angle when there are non-structural members. After that, the value decreased with increasing deformation, regardless of the amount of non-structural members.
- In the relationship between each vibration characteristics and experienced maximum drift angle, the changes in the values of steel specimens were relatively small compared with those of RC specimens. The damping values of the steel specimen is about 3 to 4%, which is about 0.7 to 0.5 times to the RC specimen, even when the drift angle reaches nearly ultimate deformation levels.

The results obtained in this study are based on a limited range of results obtained from three specimens. Moving forward, the authors hope to expand the available data by analyzing further tests.

## 7. Acknowledgements

This work was supported by JSPS KAKENHI Grant Number JP18H01588.



## 8. Copyrights

17WCEE-IAEE 2020 reserves the copyright for the published proceedings. Authors will have the right to use content of the published paper in part or in full for their own work. Authors who use previously published data and illustrations must acknowledge the source in the figure captions.

## 9. References

- [1] Architectural Institute of Japan (AIJ): *Damping in buildings*, 2000. 10 (in Japanese)
- [2] Pacific Earthquake Engineering Research Center/Applied Technology Council (PEER/ATC), 2010. Interim Guidelines on Modeling and Acceptance Criteria for Seismic Design and Analysis of Tall Buildings, *PEER/ATC-72-1*, Pacific Earthquake Engineering Research Center/Applied Technology Council, Redwood City, California.
- [3] Nakamura, N., et.al.: Study on Horizontal First Mode Vibration Characteristics of Low and Middle Rised RC and SRC Buildings Considering Amplitude Dependency, *Journal of Structural and Construction Engineering (Transactions of AIJ)*, Vol. 81, No. 721, pp. 471-481, 2016. 3 (in Japanese)
- [4] Nakamura, N., et.al.: Study on Horizontal First and Second Vibration Characteristics of High Rised Steel Buildings Considering Amplitude Dependency, *Journal of Structural and Construction Engineering (Transactions of AIJ)*, Vol. 83, No. 753, pp.1561-1571, 2018.11 (in Japanese)
- [5] National Reserch Institute for Earth Science and Disaster Resilience (NIED): <https://www.edgrid.jp/>
- [6] Tojo, T., et.al.: A Study on Vibration Characteristics of Reinforced Concrete Buildings Based on Large Shaking Table Tests, *Journal of Structural and Construction Engineering (Transactions of AIJ)*, Vol. 82, No. 741, pp. 1695-1705, 2017. 11 (in Japanese)
- [7] Tojo, T., et.al.: A Study on Vibration Characteristics of Steel Medium-Rise Buildings Based on Large Shaking Table Tests, *Journal of Structural and Construction Engineering (Transactions of AIJ)*, Vol. 83, No. 746, pp. 565-575, 2018. 4 (in Japanese)
- [8] Safak, E.: Identification of Linear Structures Using Discrete-Time Filters, *Journal of Structural Engineering*, Vol. 117, pp. 3064-3085, 1991. 10
- [9] Suita, K., et.al.: Experimental Procedure and Elastic Respose Characteristics of Shaking Table Test, *Journal of Structural and Construction Engineering (Transactions of AIJ)*, Vol. 74, No. 635, pp. 157-166, 2009. 1 (in Japanese)
- [10] Yamada, S., et.al.: Elasto-Plastic Responses and Process Leading to A Collapse Mehcanism, *Journal of Structural and Construction Engineering (Transactions of AIJ)*, Vol. 74, No. 644, pp. 1851-1859, 2009. 10 (in Japanese)
- [11] Shimada, Y., et.al.: Collapse Behavior on Shaking Table Test, *Journal of Structural and Construction Engineering (Transactions of AIJ)*, Vol. 75, No. 653, pp. 1351-1360, 2010. 7 (in Japanese)
- [12] Kasai, K., et.al.: Overall Test Outline and Response of Building without Dampers, *Journal of Structural and Construction Engineering (Transactions of AIJ)*, Vol. 76, No. 663, pp.997-1006, 2011. 5 (in Japanese)
- [13] National Reserch Institute for Earth Science and Disaster Resilience (NIED): *Experimental Study for Steel Architectural Structure Damaged by Earthquake*, 2014. 3 (in Japanese)
- [14] Kasai, K., et.al.: Evaluation Rule for Vibration Period, Damping, and Mode Vector of Buildings Tested by a Shake Table with Inevitable Rocking Motions, *Journal of Structural and Construction Engineering (Transactions of AIJ)*, Vol. 76, No. 670, pp. 2031-2040, 2011. 12 (in Japanese)
- [15] Mitsuta, M., et.al.: Shaking Table-Test Model Coupled Dynamics in E-Defense, *Transactions of the Japan Society of Mechanical Engineers Series C*, Vol. 72, No. 713, pp. 30-36, 2006. 1 (in Japanese)
- [16] Kurata, M., et.al.: Changes in Vibration Characteristics of Steel Beam-Column Connections with Composite Beams under Cyclic Loading, *Journal of Structural and Construction Engineering (Transactions of AIJ)*, Vol. 79, No.703 , pp. 1271-1278, 2014. 9 (in Japanese)
- [17] Aquino, R., et.al.: Structural Damping Estimation for Wind-Resistant Design of 200m-High Steel Office Building Using Stick-Slip Model, *Journal of Wind Engineering, JAWE*, Vol.38, No.2(No.135), pp. 35-49, 2013.4